Supplemental Information for:

Mitochondrial DNA mutation triggers early-onset intestinal epithelial cell dysfunction during acute colitis

Qian Zhang[a,b,c,1], Xiaoling Deng[a,b,c,1], Zhe Xu[b,c], Guoshi Chai[b,c], Jiatong Chen[b,c,d], Guannan Wang[e], Jia Jing[b,c], Leping Zhang[b,c], Ning Liu[b,c,d], Xiong Xiong[b,c], Yanxiao Zhang[b,c], Yanmei Dou[b,c], Min Jiang[b,c,2]

[a]Fudan University, Shanghai, China

[b]Westlake Laboratory of Life Sciences and Biomedicine, Hangzhou, Zhejiang, China

[c]School of Life Sciences, Westlake University, Hangzhou, Zhejiang, China

[d]College of Life Sciences, Zhejiang University, Hangzhou, Zhejiang, China

[e]Guangdong Institute of Gastroenterology, The Sixth Affiliated Hospital of Sun Yat-sen University, Sun Yat-sen University, Guangzhou, Guangdong, China.

[1]Q.Z. and X.D. contributed equally to this work

[2]To whom correspondence may be addressed. Email: jiangmin@westlake.edu.cn

The Supplementary file includes:

Fig. S1 to S8

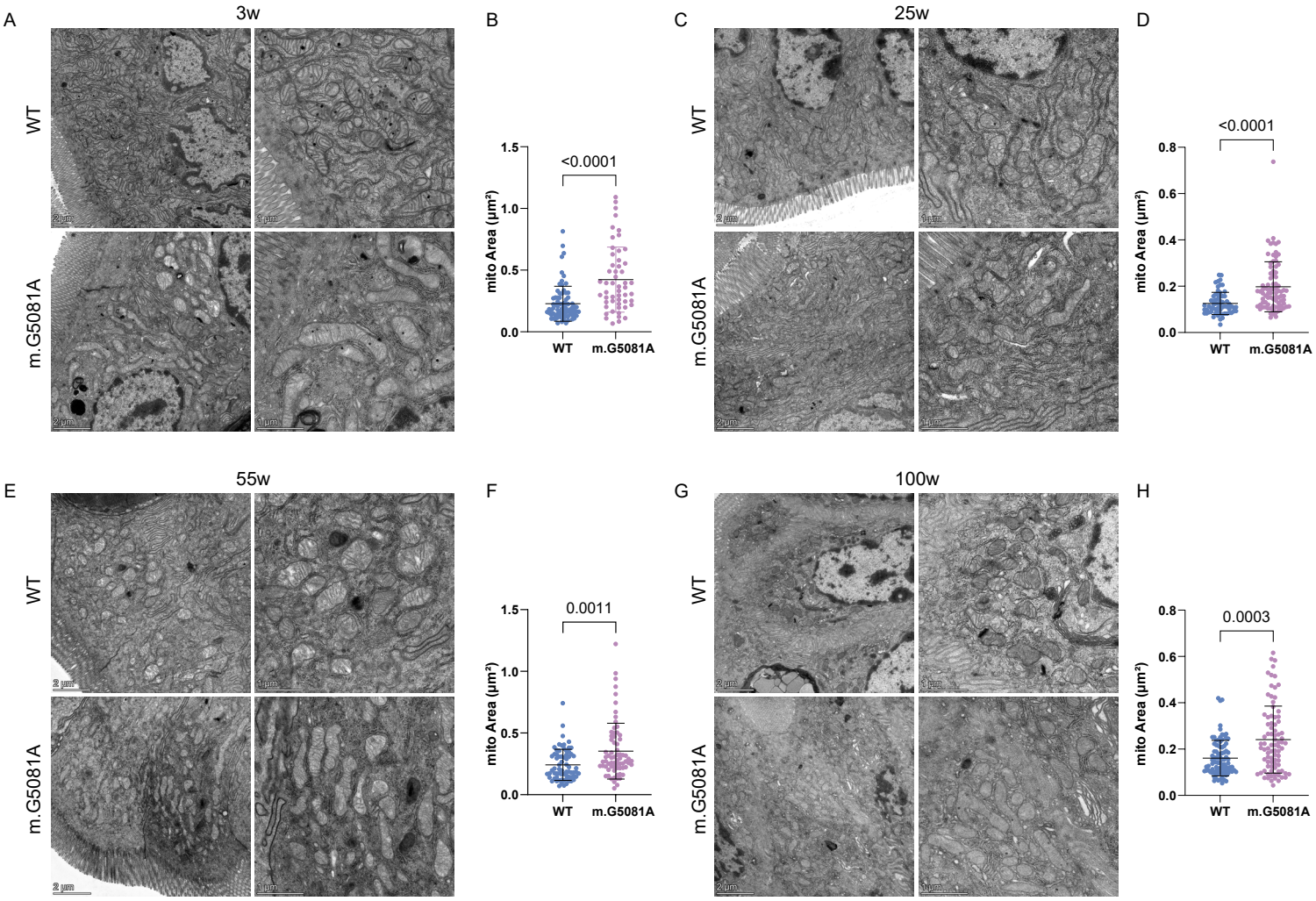

Fig. S1 The m.G5081A mutation leads to mitochondrial enlargement across all age groups.
A–H, TEM images of mitochondria and quantification of mitochondrial area in enterocytes of WT and m.G5081A mice at 3, 25, 55, and 100 weeks of age (mean ± SD, n = 3 mice per group; Mann-Whitney test).

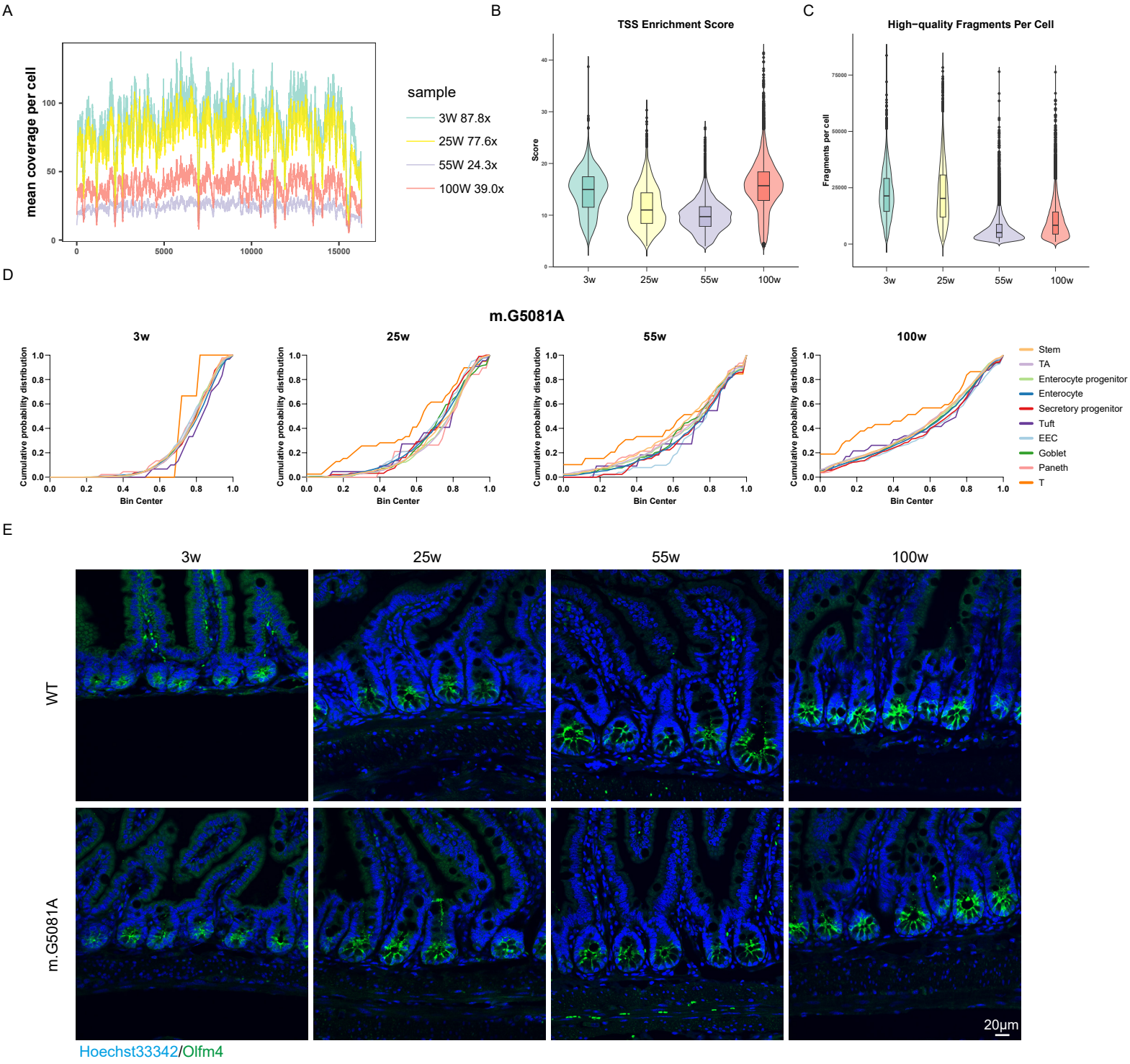

Fig. S2 Comparison of age-related selection of mtDNA mutation in m.G5081A mice.
A, Mitochondrial genome coverage profiles in 3-, 25-, 55-, and 100-week-old m.G5081A mice, with mean coverage per cell displayed.
B, Violin plot depicting TSS enrichment scores across 3-, 25-, 55-, and 100-week-old m.G5081A mice.
C, Violin plot illustrating the distribution of high-quality fragment counts in 3-, 25-, 55-, and 100-week-old m.G5081A mice.
D, Cumulative probability distribution of mitochondrial heteroplasmy levels in single cells from 3-, 25-, 55-, and 100-week-old m.G5081A mice.
E-F, Representative immunofluorescence images and quantification of Olfm4⁺ ISCs in WT and m.G5081A mice at 3, 25, 55, and 100 weeks of age (mean ± SEM, n = 3 mice per group; unpaired two-tailed Student's t-test).

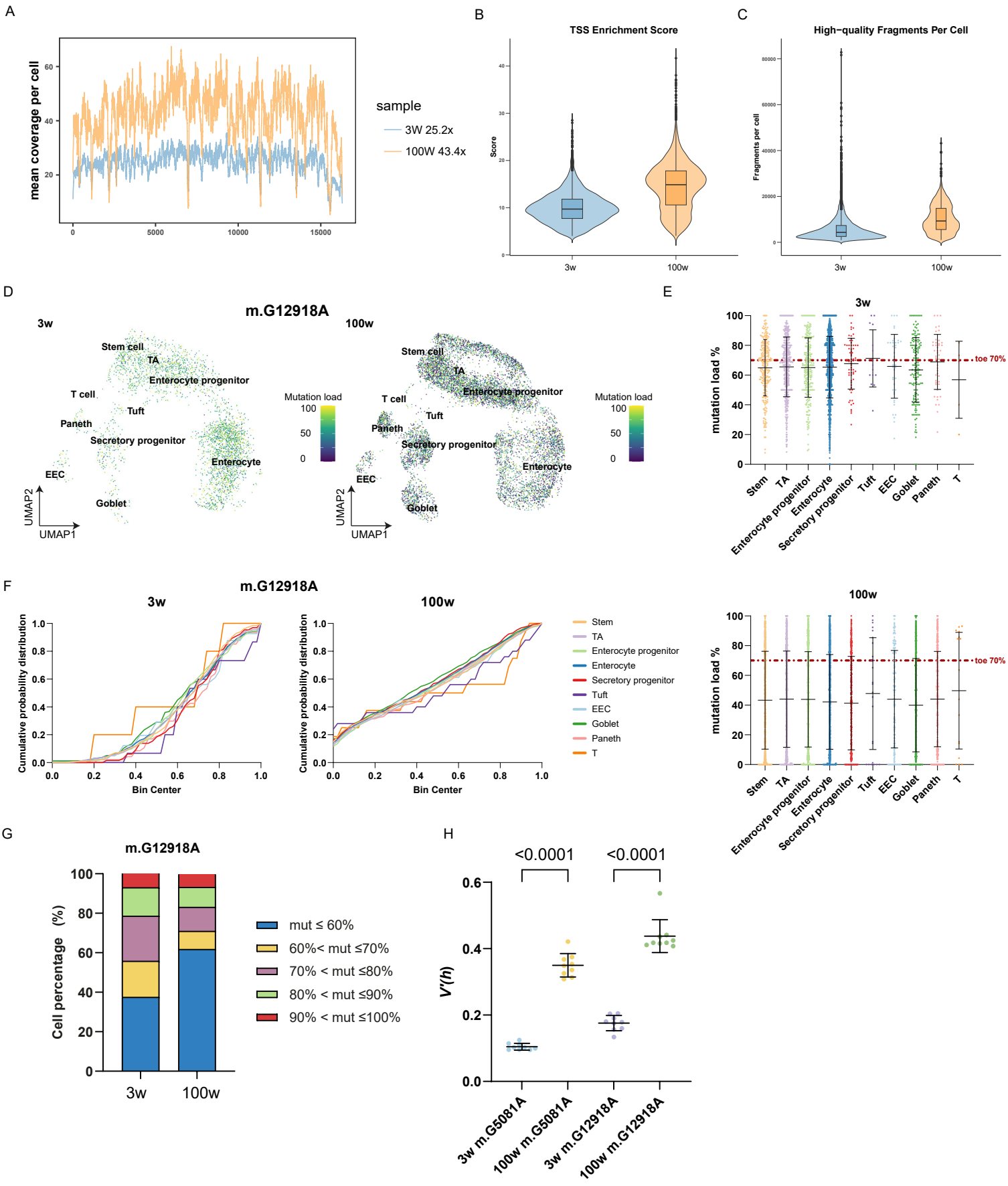

Fig. S3 Comparison of age-related selection of mtDNA mutation in m.G12918A mice.
A, Visualization of mitochondrial genome coverage in m.G12918A mice at 3 and 100 weeks of age. Mean coverage per cell is displayed.
B, Violin plot depicting TSS enrichment scores in m.G12918A mice at 3 and 100 weeks of age.
C, Violin plot showing the number of high-quality fragments in m.G12918A mice at 3 and 100 weeks of age.
D, Mutation load in IECs and T cells from 3- and 100-week-old m.G12918A mice, projected onto the UMAP from Fig. 3B.
E, Distribution of mutation load in IECs and T cells from 3- and 100-week-old m.G12918A mice.
F, Cumulative probability distribution of the heteroplasmy levels in 3- and 100-week-old m.G12918A mice.
G, The percentage of ISCs with different mutation load in 3- and 100-week-old m.G12918A groups.
H, Normalized heteroplasmy variance increases in nine IEC types from 3- and 100-week-old m.G5081A and m.G12918A mice (mean ± SD, one-way ANOVA).

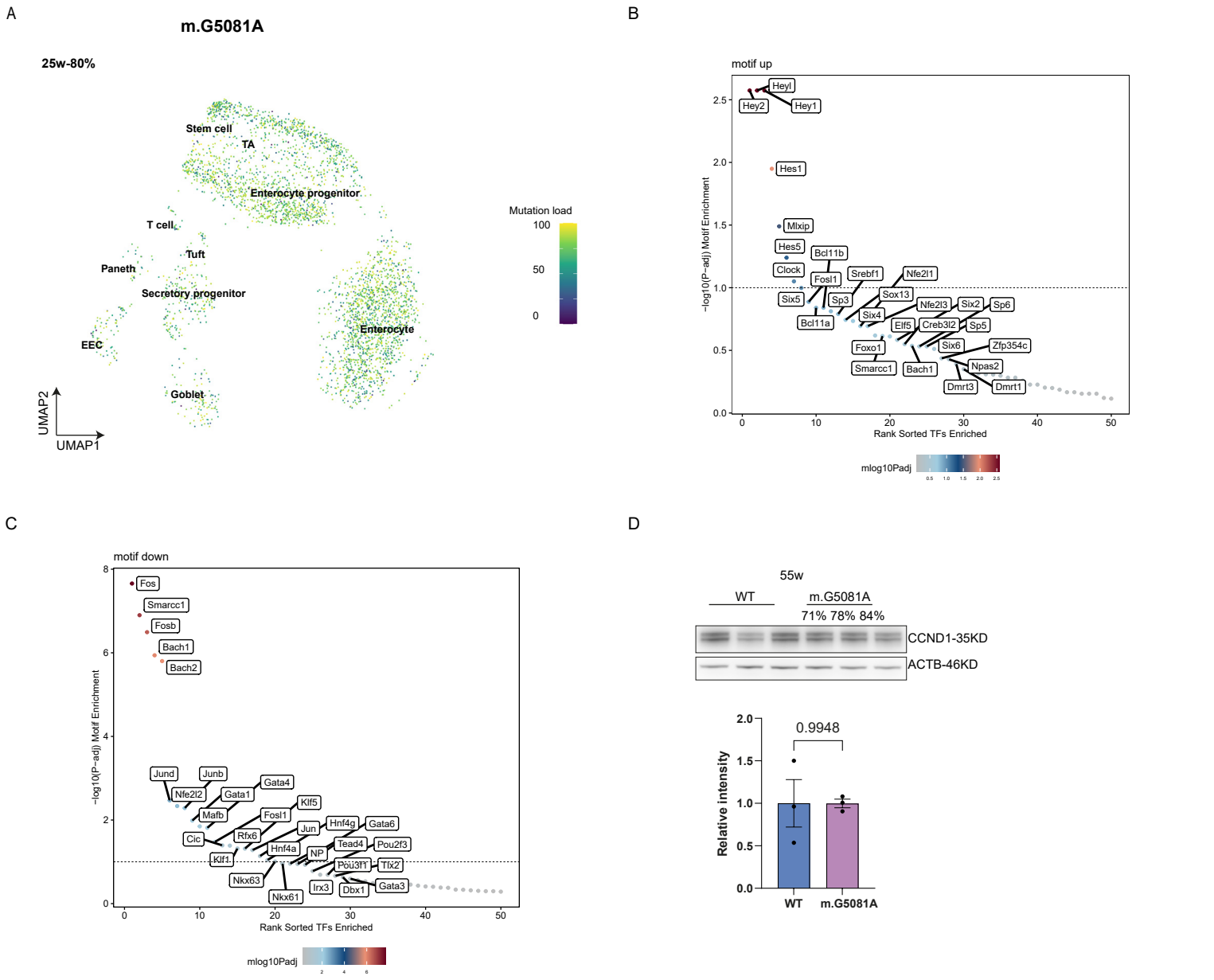

Fig. S4 The m.G5081A mutation suppresses the cell cycle progression of enterocytes in young mice.
A, Mutation load of m.G5081A in IECs and T cells from another 25-week-old mouse (toe mutation load 80%), projected onto the UMAP in panel Fig. 3B.
B-C, Upregulated and downregulated TFs in enterocytes with high mutation load (>85%) from two 25-week-old m.G5081A mice (toe mutation load 78% and 80%) compared to WT enterocytes.
D, Western blot analysis and quantification of CCND1 in IECs isolated from WT and m.G5081A mice at 55 weeks of age (mean ± SEM, n = 3 mice per group, Unpaired two-tailed Student's t-test).

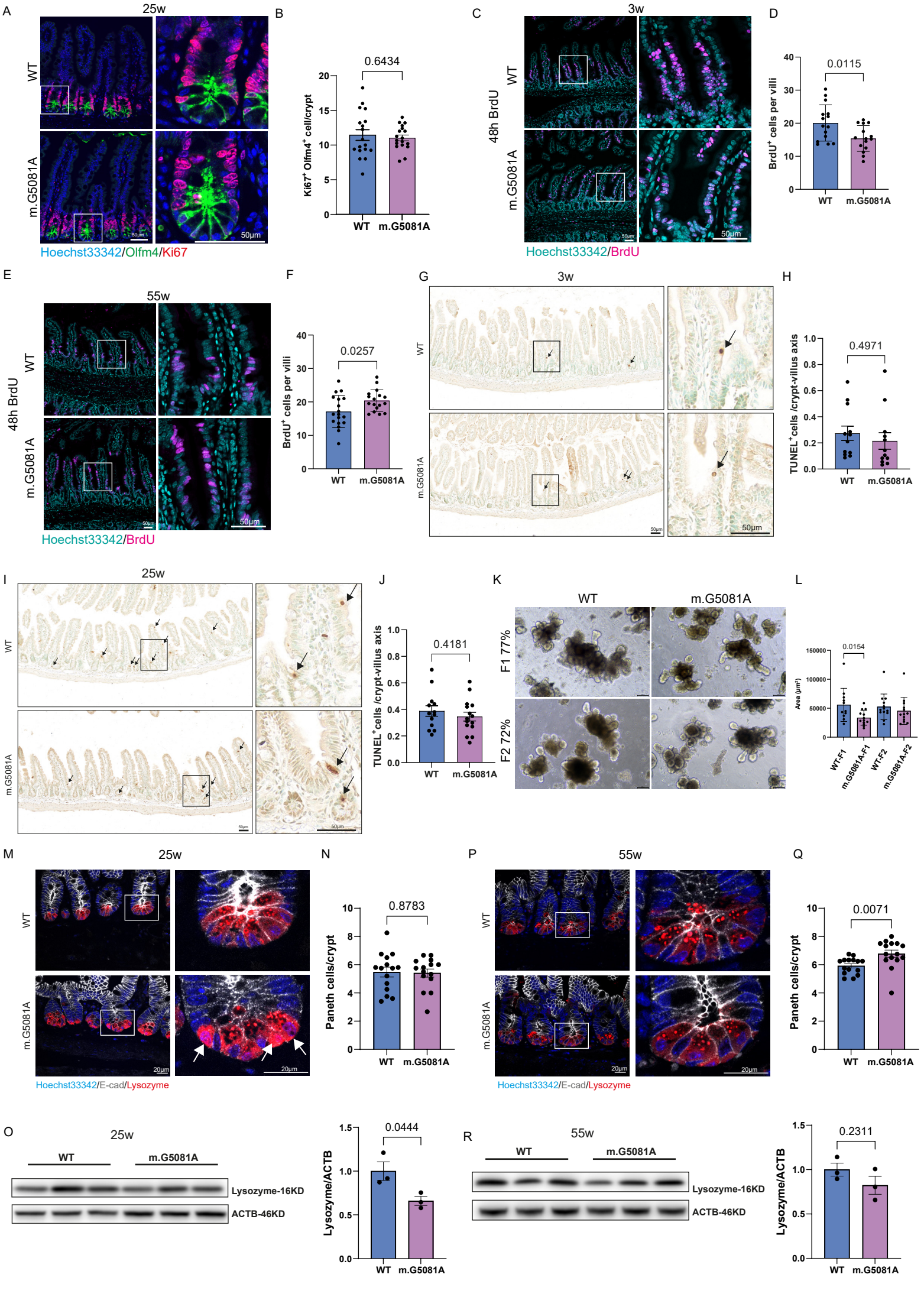
A
25w
WT
m.G5081A
50μm
Hoechst33342/Olfm4/Ki67
B
0.6434
Ki67+ Olfm4+ cell/crypt
WT
m.G5081A
C
3w
48h BrdU
WT
m.G5081A
50μm
Hoechst33342/BrdU
D
0.0115
BrdU+ cells per villi
WT
m.G5081A
E
55w
48h BrdU
WT
m.G5081A
50μm
Hoechst33342/BrdU
F
0.0257
BrdU+ cells per villi
WT
m.G5081A
G
3w
WT
m.G5081A
50μm
H
0.4971
TUNEL+cells /crypt-villus axis
WT
m.G5081A
I
25w
WT
m.G5081A
50μm
J
0.4181
TUNEL+cells /crypt-villus axis
WT
m.G5081A
K
WT
m.G5081A
F1 77%
F2 72%
L
0.0154
Area (μm²)
WT-F1
m.G5081A-F1
WT-F2
m.G5081A-F2
M
25w
WT
m.G5081A
20μm
Hoechst33342/E-cad/Lysozyme
N
0.8783
Paneth cells/crypt
WT
m.G5081A
P
55w
WT
m.G5081A
20μm
Hoechst33342/E-cad/Lysozyme
Q
0.0071
Paneth cells/crypt
WT
m.G5081A
O
25w
WT
m.G5081A
Lysozyme-16KD
ACTB-46KD
0.0444
Lysozyme/ACTB
WT
m.G5081A
R
55w
WT
m.G5081A
Lysozyme-16KD
ACTB-46KD
0.2311
Lysozyme/ACTB
WT
m.G5081A

Fig. S5 The m.G5081A mutation leads to impaired IECs function both in vivo and in vitro.
A-B, Immunofluorescence staining and quantification of $Olfm4^+$ and $Ki67^+$cells in the crypts of 25-week-old WT and m.G5081A mice (mean ± SEM, n = 3 mice per group; unpaired two-tailed Student's t-test).
C-F, Immunofluorescence staining and quantification of BrdU-labeled cells in the small intestine of 3-week-old (C, D) and 55- week-old (E, F) WT and m.G5081A mice 48 hours after BrdU administration (mean ± SD, n = 3 mice per group; unpaired two-tailed Student's t-test).
G-J, Representative images and quantification of TUNEL-positive IECs in the intestinal sections from 3-week-old (G, H) and 25-week-old (I, J) WT and m.G5081A mice (mean ± SEM, n = 3 mice per group; unpaired two-tailed Student's t-test).
K-L, Representative images and quantification of F1 and F2 organoid area derived from WT and m.G5081A mice (mean ± SD, n ≥ 11 organoids; Mann-Whitney test).
M-O, Immunofluorescence staining for Lysozyme (arrows indicate the defective Paneth cells without granules) and quantification of Paneth cells in the small intestine of 25-week-old (M, N) and the detection and quantification of Lysozyme level of IECs by Western blot (O). (mean ± SEM, n = 3 mice per group; unpaired two-tailed Student's t-test).
P-R, Immunofluorescence staining for lysozyme and quantification of Paneth cells in the small intestine of 55-week-old (P, Q) and the detection and quantification of Lysozyme level of IECs by Western blot (R). (mean ± SEM, n = 3 mice per group; unpaired two-tailed Student's t-test).

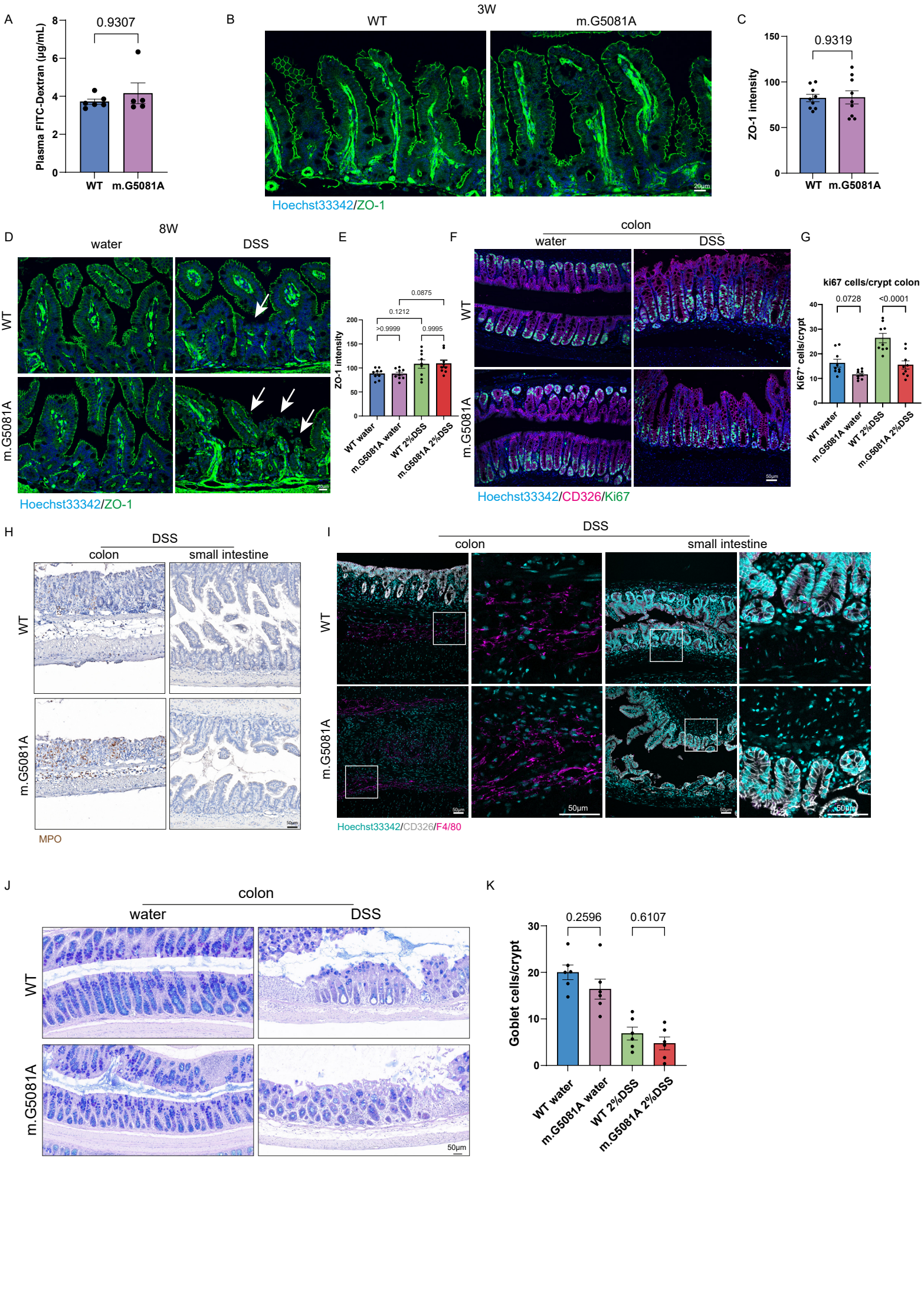
A
0.9307
Plasma FITC-Dextran (μg/mL)
WT
m.G5081A
B
3W
WT
m.G5081A
20μm
Hoechst33342/ZO-1
C
0.9319
ZO-1 intensity
WT
m.G5081A
D
8W
water
DSS
WT
m.G5081A
Hoechst33342/ZO-1
E
0.0875
0.1212
>0.9999
0.9995
ZO-1 intensity
WT water
m.G5081A water
WT 2%DSS
m.G5081A 2%DSS
F
colon
water
DSS
WT
m.G5081A
50μm
Hoechst33342/CD326/Ki67
G
ki67 cells/crypt colon
0.0728
<0.0001
Ki67+ cells/crypt
WT water
m.G5081A water
WT 2%DSS
m.G5081A 2%DSS
H
DSS
colon
small intestine
WT
m.G5081A
50μm
MPO
I
DSS
colon
small intestine
WT
m.G5081A
50μm
Hoechst33342/CD326/F4/80
J
colon
water
DSS
WT
m.G5081A
50μm
K
0.2596
0.6107
Goblet cells/crypt
WT water
m.G5081A water
WT 2%DSS
m.G5081A 2%DSS

Fig. S6 The erosion of epithelial cells disrupted the intestinal barrier and did not elicit an immune response in the small intestine.
A, Concentration of 4-kDa FITC dextran in plasma of young (5-8 weeks old) WT and m.G5081A mice (mean ± SEM, n > 3 mice per group; Mann-Whitney test).
B-C, Immunohistochemical staining for ZO-1 in IECs and quantification of ZO-1 expression in small intestine sections from 3- week-old WT and m.G5081A mice (mean ± SEM, n = 3 mice per group; unpaired two-tailed Student's t-test).
D-E, Immunohistochemical staining for ZO-1 and quantification of ZO-1 expression in small intestine sections from 8-week-old WT and m.G5081A mice treated with water or DSS (mean ± SEM, n ≥ 3 mice per group; one-way ANOVA). The arrow indicated the eroded epithelium under DSS treatment.
F-G, Immunofluorescence staining for $CD326^+$ and $Ki67^+$ cells in colon from WT and m.G5081A mice after water or DSS treatment, with quantification of $Ki67^+$ cells in the colon (mean ± SEM; n = 3; one-way ANOVA).
H, Immunohistochemical staining for MPO (neutrophils) in colon and small intestine sections from WT and m.G5081A mice following DSS treatment.
I, Immunofluorescence staining for CD326 (epithelial cells) and F4/80 (macrophages) in colon and small intestine sections from WT and m.G5081A mice after DSS treatment.
J-K, AB-PAS staining and quantification of goblet cells in the colon from WT and m.G5081A mice after DSS treatment (mean ± SEM; n = 3; one-way ANOVA).

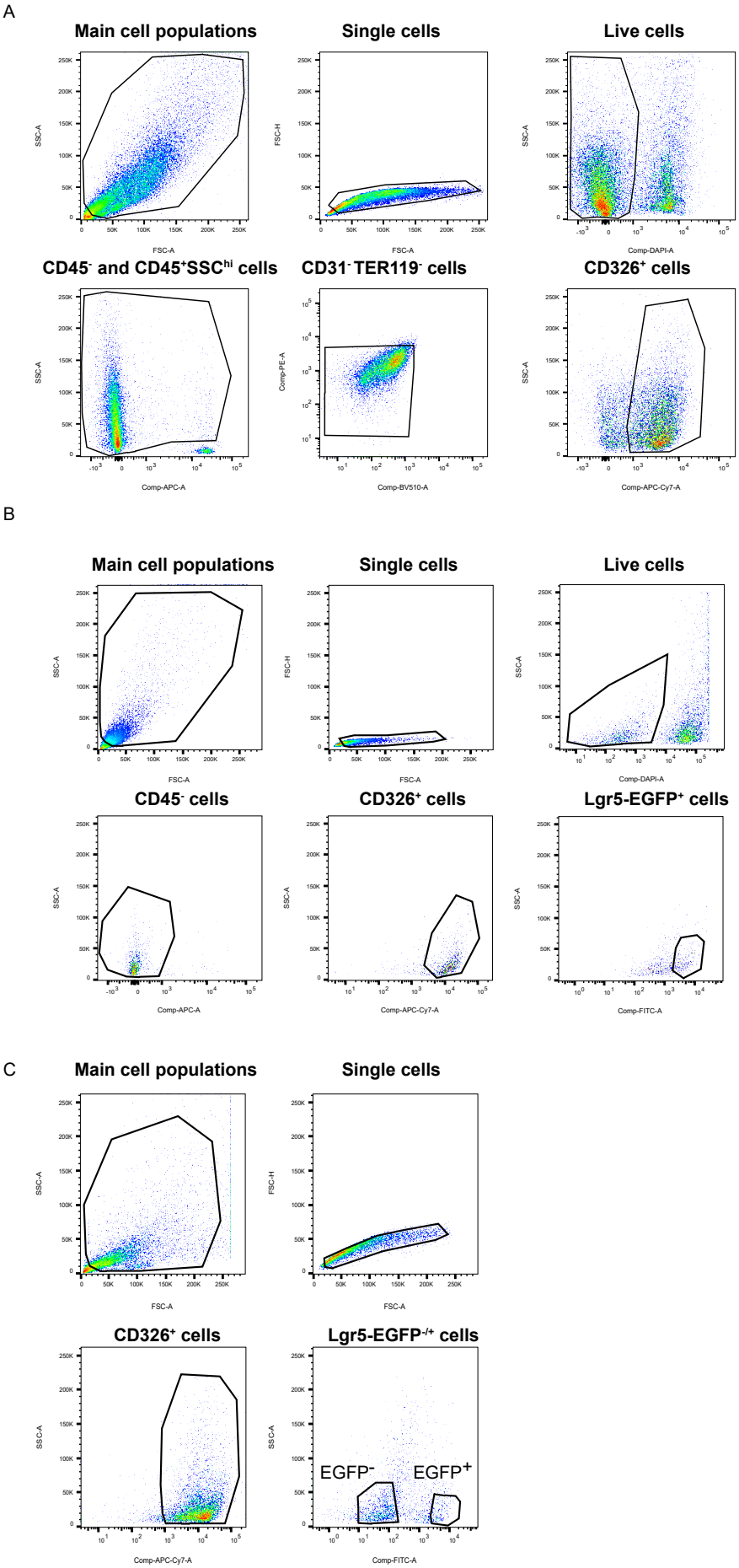

Fig. S7 The gating strategy of epithelial cells.

A, The first gate is used to exclude debris via FSC-A and SSC-A, followed by doublet exclusion using FSC-A and FSC-H. DAPI$^-$ cells were chosen as live cells. CD45$^+$ SSC^{low} cells were excluded as immune cells. CD31$^-$ TER119$^-$ cells were used to exclude platelet endothelial cells and erythroid cells. Finally, CD326$^+$ cells were sorted for further analysis.

B, The first gate is used to exclude debris via FSC-A and SSC-A, followed by doublet exclusion using FSC-A and FSC-H. DAPI$^-$ cells were chosen as live cells. CD45$^-$ and CD326$^+$ cells were used to isolate Lgr5-EGFP$^+$ ISCs for organoid culture.

C, The first gate is used to exclude debris via FSC-A and SSC-A, followed by doublet exclusion using FSC-A and FSC-H. DAPI$^-$ cells were chosen as live cells. CD326$^+$ cells were used to isolate single Lgr5-EGFP$^+$ ISCs and Lgr5-EGFP$^-$ IECs for mutation load detection.

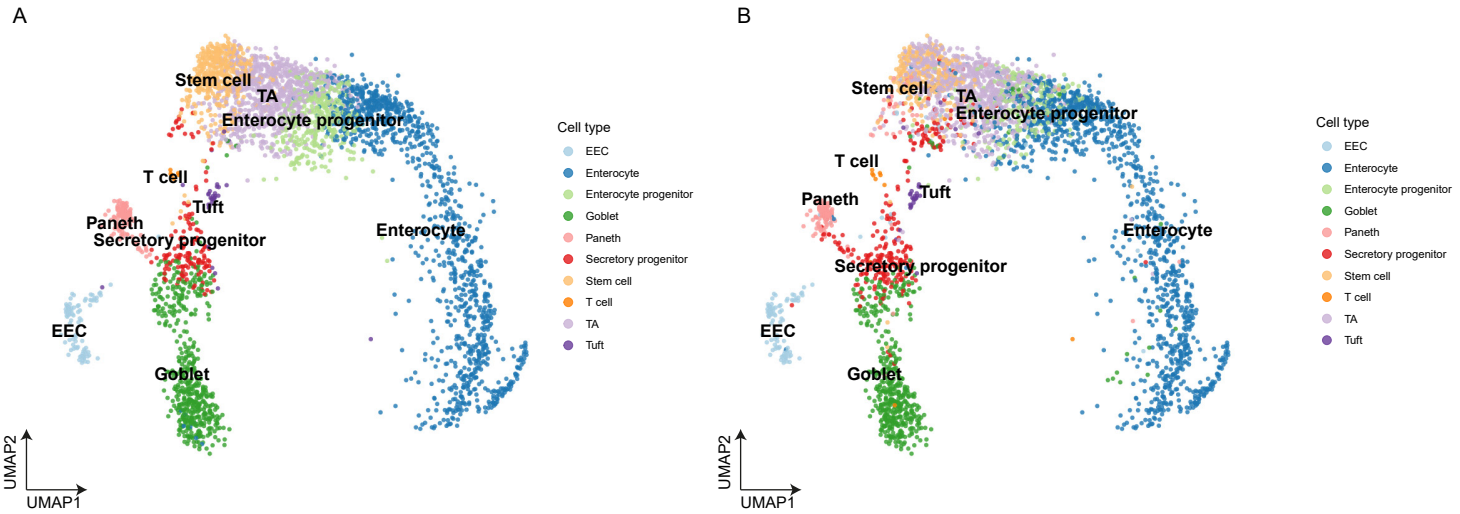

Fig. S8 Cell annotation of mtscATAC-seq.
A, The annotation of cells based on scRNA-seq data.
B, The annotation of cells based on the shared barcode of Multiomic data.